energy&fuels

Study of the Chemical Structure of Laminar Premixed H_2/CH_4/C_3H_8/O_2/Ar Flames at 1−5 atm

D. A. Knyazkov,*[†,‡] A. M. Dmitriev,[†,§] V. M. Shvartsberg,[†] K. N. Osipova,[†,§] A. G. Shmakov,[†,§] and O. P. Korobeinichev[†]

[†]Institute of Chemical Kinetics and Combustion, Novosibirsk 630090, Russia

[‡]Far Eastern Federal University, Vladivostok 690950, Russia

[§]Novosibirsk State University, Novosibirsk 630090, Russia

ABSTRACT: The paper presents an experimental and modeling study of the chemical structure of laminar premixed stoichiometric H_2/CH_4/C_3H_8/O_2/Ar flames stabilized on a flat burner at 1, 3, and 5 atm. The flame structure was simulated using four different detailed chemical kinetic mechanisms proposed in the literature for oxidation of small hydrocarbons. The width of the zone of consumption of the fuel components was shown to differ appreciably at the three pressures. Hydrogen was shown to have the largest consumption zone, while propane has the smallest one. The kinetic analysis provided an explanation for the observed phenomenon, which assumes the formation of additional pathways for hydrogen and methane production in the flames of ternary fuel mixtures. Comparison of the measured and simulated flame structures shows that all the mechanisms satisfactorily predict the mole fraction profiles of the reactants, products, and some intermediates at atmospheric and elevated pressures. It is noteworthy that the mechanisms adequately predict the spatial variations in the mole fractions of free radicals, including the H, OH, and CH_3 radicals, within the pressure range. However, some drawbacks of the mechanisms used have been identified. The mechanisms were shown to overpredict the mole fractions of some unsaturated hydrocarbons, including ethylene and acetylene, at elevated pressures. Therefore, the rate constants of the crucial reactions responsible for production/consumption of these species, as well as their pressure dependences, should be specified, and the mechanisms should be refined. To provide a deeper insight into the combustion chemistry of ternary fuel mixtures, one should focus on the structure of rich flames.

■ INTRODUCTION

Natural gas is widely used in the electric power industry and in thermal power production as fuel for gas turbines and steam boilers and in transport. Natural gas has an advantage over coal and oil products as its use produces significantly less hazardous emissions; in addition, natural gas has a higher detonation resistance and a comparatively low cost.[1,2] Although natural gas mostly consists of methane, it may also include heavier hydrocarbons: from C_2H_6 to C_6H_{14}. The percentage of hydrocarbons in produced natural gas depends on the gas field and on the season.[3] Therefore, it is necessary to carry out a thorough study of the combustion of blended fuels containing not only methane but also heavier hydrocarbons, as the composition of these fuels is always crucial for their combustion and ignition. On the other hand, the addition of hydrogen (or syngas) to conventional hydrocarbon fuels is a promising method for improving the characteristics of combustion processes in internal combustion engines. Addition of 20−30% hydrogen to hydrocarbons[4] extends the concentration limits of combustion (which is especially important for clean fuels[5]), makes their ignition easier, and reduces the temperature of the final combustion products. Therefore, adding hydrogen to compressed or liquefied natural gas is considered to be a relatively simple method for reducing emission of carbon-containing compounds and NO_x in the exhaust of internal combustion engines. Combustion of blended fuels consisting of hydrogen and hydrocarbons is of great interest to researchers, as the mutual influence of these compounds on the chemistry

and kinetics of the oxidation processes has not been sufficiently investigated, especially at elevated pressures close to the pressures in actual internal combustion engines.

Combustion of binary mixtures of hydrogen and methane or propane has been studied most thoroughly. In most studies of the combustion of hydrogen−hydrocarbon mixed fuels, the flame speeds for such fuels mixed with air have been measured. In addition, in a few papers, autoignition delays in shock tubes and oxidation in a flow reactor have been investigated. These studies have shown that adding hydrogen to hydrocarbons accelerates the combustion process of such a blended fuel and, in contrast, adding hydrocarbons slows down the combustion of hydrogen. It is important to note that, according to the available experimental data on flame speed, Le Chatelier's principle does not usually work; i.e., the flame speed in H_2 + C_xH_y fuel mixtures increases nonlinearly as the hydrogen concentration varies from 0 to 100%. This suggests that the combustion processes of hydrogen and hydrocarbons mutually influence each other and cannot be considered separately. If measurements of the flame speed are performed in a sufficiently narrow range of H_2 concentration in a H_2 + C_xH_y mixture, the effect of changing the H_2 concentration change will be described by a nearly linear relation.

A

Such observations are described, for example, in ref 6. In measuring the flame speed at atmospheric pressure in the counterflow configuration, the authors of this study found that addition of hydrogen to methane−air and propane−air flames resulted in a considerable increase in their speed. The flame speed was found to depend linearly on the hydrogen addition in the range of its concentration up to 50% for methane flames and up to 25% for propane flames. Similar results were also obtained for mixtures of natural gas with hydrogen and air (equivalence ratio (ϕ) = 0.6−1.4) at a pressure of 1 atm and an initial temperature of 300 K.[7] At the same time, Hu et al.[8] measured the flame speed of H_2 + CH_4/air mixture at atmospheric pressure. It was shown that, at a hydrogen concentration in the fuel exceeding 60%, the dependence of the flame speed changes nonlinearly as the H_2 concentration increases to 80%. Above this concentration, the dependence of the flame speed becomes linear again. Similar results were obtained in studies[9] of the laminar flame speed of methane/hydrogen/air mixtures at 1 atm. Using the heat flux method,[10,11] Konnov et al.[12−17] measured the flame speed of methane/air mixtures with H_2 and/or CO_2 additives with the H_2 concentration in H_2/CH_4 mixtures being 40% or lower. The equivalence ratio was varied in the range ϕ = 0.8−1.4 and the pressure was 20−100 kPa. Hermanns et al.[14] determined that dependence of H_2 + CH_4 + air flame speeds on the composition and the initial temperature in the H_2 concentration range from 0 to 50% can be described by relatively simple empirical relations. However, at higher hydrogen concentrations, simple dependences were not obtained.

Similar conclusions have been also made in ref 18. The authors proposed a theoretical model for evaluating the flame speed of binary hydrogen and methane mixtures based on the data describing the speed of individual mixtures of these fuels with air. It was established that, in H_2 + CH_4 mixtures in the H_2 concentration range from 0 to 50% and from 90 to 100%, the flame speed increased linearly with increasing percentage of H_2. However, when the H_2 concentration grew from 50 to 90%, the flame speed increased nonlinearly. Chen et al.[19] proposed an improved method for evaluating the flame speed of hydrogen/methane mixtures. In this method, calculation is conducted using not only data on the flame speed of individual fuels but also data on the speed of binary mixtures of H_2 + CH_4 with air.

It is interesting to note that, according to the available data, adding hydrogen to different hydrocarbons differently affects their oxidation. For example, Park et al.[20] studied combustion of H_2 + CO + CH_4 and H_2 + CO + C_3H_8 mixtures at 1−4 atm by measuring the flame speed in a counterflow configuration. In accordance with their data, replacement of part of CH_4 with C_3H_8 in the mixtures considerably decreased the flame speed. Kinetic analysis showed that this effect may be related to the high concentration of CH_3 radicals (which are formed to a greater extent from C_3H_8 than from CH_4). This eventually leads to a reduction in the H concentration due to their recombination with CH_3, which, in turn, decreases the net rate of the chain-branching reaction H + O_2 ↔ O + OH.

In accordance with the majority of the literature data, no crucial changes are observed in the dependence of the flame speed of H_2 + C_xH_y mixtures on the pressure and/or temperature. Okafor et al.[21] used a constant-volume fan-stirred combustion chamber to measure the dependence of the flame speed of H_2 + CH_4 + air mixtures (ϕ = 0.8, 1.0, and 1.2) with the H_2 concentration in the fuel mixture varying from 0 to 100% at 1 atm at an initial temperature of 350 K. . It was

established that the flame speed depended nonlinearly on the hydrogen concentration in H_2/CH_4 mixtures for all values of ϕ. In a similar way, the flame speed was measured in a C_3H_8 + O_2 + He + H_2 mixture (ϕ = 0.6) at 20 atm and an initial temperature of 298 °C.[22] Although the authors stated that they observed a linear dependence of the flame speed versus H_2 fraction in the range from 0 to 35% in the mixture with propane, according to ref 22, it is clear that this dependence is not quite linear. Vu et al.[23] measured the speed of CH_4/H_2/CO/air and C_3H_8/H_2/CO/air flames (ϕ = 0.8−1.2) at pressures of 1−4 atm and an initial temperature of 298 °C. It was shown the flame speed also increased nonlinearly as the fraction of H_2 was raised. Using a constant-volume fan-stirred combustion chamber, Donohoe et al.[24] measured the speed of H_2/CH_4/O_2/He flames (ϕ = 0.7−1.3), with an H_2 fraction of 50−90% in the mixture with CH_4 at 1−5 atm and in an initial temperature range from 300 to 450 K. . As in the other studies, the flame speed increased nonlinearly as the fraction of hydrogen in the fuel mixture was increased. Halter et al.[25] showed that, at higher pressures (3 and 5 atm), addition of hydrogen (the mole fraction of H_2 in the fuel was varied from 0 to 0.2) resulted in a nonlinear growth in the speed of CH_4 + H_2−air flames, whereas at atmospheric pressure the flame speed in such mixtures increased linearly with increasing concentration of the hydrogen additive. Thus, in contrast to the other studies, Halter et al.[25] demonstrated that a change in the pressure affected the behavior of the flame speed at various fractions of hydrogen in the fuel. This may indicate that, under these conditions, there is a change in the mechanism of interplay between the H_2 and CH_4 oxidation process.

However, addition of hydrogen not only increases the flame speed of hydrocarbon mixtures, but also affects the parameters of their autoignition. For example, Petersen et al.[26] used a shock tube to investigate the autoignition of lean (ϕ = 0.5) CH_4/H_2 mixtures (80/20% and 60/40%) at 18−25 atm and a temperature of 1140−1550 K. Addition of hydrogen to methane was shown to result in 3-fold and 10-fold reductions in the autoignition delays at 20 and 40% H_2, respectively, in the mixture with CH_4. The authors note that addition of 20−40% hydrogen does not significantly change the activation energy of autoignition of the methane/hydrogen mixture compared to pure methane. In the previously mentioned study,[24] mixtures of natural gas with hydrogen were studied at 1, 10, and 30 atm. Natural gas was simulated by mixtures of C_1/C_2/C_3/C_4/C_5 hydrocarbons of compositions 81.25/10/5/2.5/1.25 and 62.5/20/10/5/2.5. Using a shock tube and a rapid compression machine, autoignition delays were measured in hydrocarbon mixtures with 30, 60 and 80% H_2 additives in the temperature range 850−1800 K and at ϕ = 0.3−1. The autoignition delay time was shown to reduce with increasing fraction of hydrogen. Similar results were obtained by Zhang et al.[5] for H_2/CH_4/O_2/Ar mixtures in a shock tube at 5−20 atm and temperatures of 1000−2000 K. The authors also ascertained that adding hydrogen promotes the combustion of methane or decreases the autoignition temperature (at fixed ignition time) or decreases the autoignition delay (at fixed temperature). When the fraction of hydrogen in a CH_4 + H_2 mixture increases, the dependence of autoignition delays on temperature differs drastically from the two limiting cases (pure methane and pure hydrogen). For pure methane, as the pressure grows, the autoignition delay decreases (in the temperature range 1250−2000 K). For pure hydrogen, increasing the pressure results in a prolonged autoignition delay (in the range of temperatures

1000−1250 K). In a 60% H_2 and 40% CH_4 mixture, the autoignition delay does not depend on the pressure, indicating a complex interaction between the oxidation reactions of H_2 and CH_4 in this system. Kinetic analysis of the calculated autoignition delays of $H_2/CH_4/O_2/Ar$ mixtures showed that, in this system, the promoting impact of hydrogen can be attributed to the increased concentration of H, O, and OH in the reacting mixture.

The promoting effect of hydrogen on hydrocarbon oxidation was also observed by Dagaut and Nicolle.[27] They investigated the oxidation of hydrocarbon/H_2/air mixtures (ϕ = 0.3, 1, 2) in a jet-stirred reactor at 1 atm in the temperature range 900−1450 K. A $CH_4/C_2H_6/C_3H_8$ (89.3%/8.9%/1.8%) mixture simulated natural gas into which hydrogen was introduced (volume fraction was 40 or 75%). Addition of 40 and 75% hydrogen (at constant ϕ) reduced the characteristic temperature corresponding to the peak concentrations of CO and C_2H_4 (intermediate products of fuel oxidation) by 100 and 200 K, respectively. This effect was especially pronounced for lean mixtures. The observed effect, according to the authors, is related to the fact that increasing the initial fraction of hydrogen increased the concentration of HO_2 radicals, which finally produced hydroxyl: $HO_2 + H \leftrightarrow H_2O_2$; $H_2O_2 + M \leftrightarrow OH + OH$. As low-temperature oxidation of hydrogen and hydrocarbons occurs mainly in reactions with OH, these reactions generally accelerate the fuel oxidation. Dagaut and Dayma[28] also found the promoting effect of oxidation of a CH_4/C_2H_6 mixture (10:1) by an H_2 additive under elevated pressure. Just as in ref 27, at a pressure of 10 atm, replacement of 40 and 75% of CH_4/C_2H_6 mixture with hydrogen resulted in decreases of 50 and 100 K, respectively, in the temperature corresponding to the maximum emission of C_2H_4 in the products. Analysis of the results of numerical modeling has shown the promoting effect to be related to an increase in the concentration of OH radicals, determining the rate of low-temperature oxidation.

Investigation of the chemical flame structure is the most informative approach to the study of the impact of a hydrogen additive on the mechanism of reactions in hydrocarbon/air flames. De Ferrieres et al.[29] investigated the structure of $CH_4/C_2H_6/C_3H_8/O_2/N_2$ flames (ϕ = 0.74, 1.0) (mixtures simulating natural gas) without and with 20 and 60% H_2, stabilized on a flat burner at 0.079 atm. Using microprobe sampling, followed by gas chromatography analysis and Fourier transform infrared spectroscopy, the authors measured the concentration profiles of stable species, including the reactants CH_4, C_3H_8, H_2, and O_2, the final products CO_2, CO, and H_2O, and stable intermediates C_2H_2, C_2H_4, and C_3H_6. The authors also carried out numerical simulation of the investigated flames using different mechanisms and analyzed the reaction pathways. Consequently, it has been found that hydrogen addition to lean hydrocarbon flames increases the reaction rate of hydrogen abstraction from different hydrocarbon molecules, thus raising their oxidation rate. As a result, the concentration of hydrocarbons, which are soot precursors, in the flame becomes significantly lower.

De Ferrieres et al.[30] investigated the influence of a 60% hydrogen additive on the combustion of a $CH_4/C_2H_6/C_3H_8$ mixture both experimentally and numerically. The lean flames of these mixtures with O_2 and N_2 (ϕ = 0.74) were stabilized on a flat burner at 1 atm. The flames were sampled with a quartz microprobe, and the composition of the samples was analyzed by chromatography−mass spectrometry, gas chromatography, and Fourier transform infrared spectroscopy. The results obtained demonstrated that, just as in the flame of natural gas at low pressure,[29] at a pressure of 1 atm, addition of H_2 led to acceleration of the oxidation of C_1 hydrocarbons due to the increased contribution of the recombination reaction H + C_2H_5 involving CH_3 formed. This explains the decrease in the concentrations of C_2H_2 and C_2H_4 in the flame of natural gas with addition of 60% H_2.

At the same time, addition of hydrogen to very rich methane flames may lead to an increase in the concentration of C_2−C_7 hydrocarbons, which are precursors of polycyclic aromatic hydrocarbons (PAH) and soot.[31] Replacement of 40% CH_4 by H_2 in rich flames (ϕ = 2.2−2.42) at 1 atm resulted in a considerable increase in the concentrations of C_2−C_7 hydrocarbons in both the reaction zone and the postflame zone. This study demonstrates that the effect of the H_2 additive on the concentration of intermediate combustion products that are precursors of PAH and soot may depend on specific conditions such as the fuel/oxidant ratio, the coefficient of dilution of the fuel mixture with inert gas, initial temperature, pressure, etc.

Thus, the above literature survey shows that, despite the numerous experimental and modeling studies of combustion of multicomponent gas mixtures containing hydrogen, methane, and other hydrocarbons, the process of mutual influence of the components of these mixtures is not sufficiently clear. Although data on the flame structure provide most of the information on the elementary processes occurring in the flames and thus serve as a basis for validating proposed kinetic models of fuel combustion, such data in the literature are limited. Moreover, they have been obtained at low and atmospheric pressures, whereas the flame structure of such mixtures at elevated pressures has not been investigated at all. This was the main motivation for our present study. The goals of this study were the following: (1) to obtain experimental data on the chemical structure of $H_2/CH_4/C_3H_8/O_2/Ar$ flames stabilized on a flat burner at pressures from 1 to 5 atm using molecular-beam mass spectrometry (MBMS) with soft electron ionization, allowing identification and measurement of mole fractions of labile combustion products, including atoms and radicals; (2) to perform numerical simulation of the structure of these flames using four detailed chemical kinetic mechanisms for combustion of small hydrocarbons; (3) to reveal the deficiencies of the kinetic mechanisms by comparing the experimental and modeling results, and by analyzing the production and consumption reaction pathways of the fuel components and some key intermediates.

■ EXPERIMENTAL DETAILS

The chemical structures of the flames of hydrogen/methane/propane/oxygen/argon mixtures at 1, 3, and 5 atm were examined using a quadrupole mass spectrometer with a molecular-beam sampling system and electron ionization. Although the experimental setup, experimental methodology, and procedure of the experimental data reduction have been described in detail in our previous papers,[32,33] a brief description of these is provided below.

Laminar flames of premixed stoichiometric $H_2/CH_4/C_3H_8/O_2/Ar$ mixtures were stabilized on Botha−Spalding-type burners.[34] Atmospheric-pressure flames were stabilized on a burner with a perforated brass matrix 16 mm in diameter. The matrix was 3 mm thick, the diameter of the holes was 0.5 mm, and the spacing between the hole centers was 0.7 mm. For experiments at elevated pressures (3 and 5 atm), we used a burner with a perforated brass matrix 6 mm in diameter and 2 mm thick with a hole diameter of 0.2 mm and a hole center-to-center spacing of 0.26 mm. The burners could be moved in the vertical direction with the help of a micrometer screw mechanism.

326 The distance between the burner surface and the probe tip was
327 measured with a cathetometer with an accuracy of up to ± 0.01 mm.
328 To stabilize the flames at 3 and 5 atm, the burner was placed in a high-
329 pressure chamber, which was pressurized with nitrogen throughout the
330 experiment. The chamber was designed to operate at pressures of up
331 to 10 atm. It was equipped with a lateral flange for a window which
332 provided optical access for operator view. Nitrogen for pressurizing the
333 chamber was supplied through the inlet in this flange to prevent
334 condensation of water on the window and therefore to provide its
335 transparency during the experiment. The pressure in the chamber was
336 regulated with a diaphragm pressure regulator on the exhaust line and
337 was maintained at a set level with an accuracy of up to 1%. The
338 chamber was also equipped with a safety valve and a gauge for pressure
339 control. The top flange of the high-pressure chamber was connected to
340 the sampling probe flange of the molecular-beam mass spectrometric
341 setup.

342 The composition of the fresh mixture and the conditions of flame
t1 343 stabilization are shown in Table 1. The linear velocities of the fresh

Table 1. Molar Composition of Fresh Mixtures and Conditions of Stabilization of $H_2/CH_4/C_3H_8/O_2/Ar$ Flames

| press. (atm) | ϕ | reactant mole fraction | | | | | gas mixture velocity at burner surf. (cm/s) |
		H_2	CH_4	C_3H_8	O_2	Ar	
1	1.0	0.019	0.019	0.019	0.143	0.8	23.2
3	1.0	0.019	0.019	0.019	0.143	0.8	39.2
5	1.0	0.019	0.019	0.019	0.143	0.8	23.5

344 mixture above the burner at different pressures were chosen so that the
345 flames were visually flat and stable at a certain pressure and so that the
346 temperature values in the postflame zone were as close to each other
347 as possible. This allowed us to minimize the effect of the burning
348 temperature on the chemical kinetic processes in the flames at different
349 pressures and thus to analyze more accurately the pressure effect on
350 the flame structure. The mass flow rates of the fresh gas mixture
351 components were set with mass flow controllers (MKS Instruments
352 Inc.). The burner temperature was maintained at 348 K with water
353 supplied by a thermostat into the cooling jacket of the burner.

354 Flames were sampled with a conical quartz probe with an internal
355 opening angle of 40° and a tip orifice diameter of 0.04 mm. The wall
356 thickness of the probe near the tip was 0.08 mm, which allowed the
357 thermal perturbation of the flame by the probe to be minimized. The
358 freely expanding gas jet in the probe was skimmed into a molecular
359 beam, which, having passed through a modulator and a collimator,
360 entered the electron ionization region. Using soft ionization (electron
361 scattering energy of ± 0.25 eV) allowed us to neglect the contributions
362 of fragment ions to most of the measured mass peaks, which
363 significantly alleviated the identification of the combustion products.
364 The energy of electrons was selected individually for each species
365 analyzed in order to obtain a sufficiently high signal-to-noise ratio and
366 prevent interferences caused by fragmentation of other species. The
367 species whose mole fraction profiles were measured in this study are
368 shown in Table 2. Table 2 also lists their ionization energies, the t2
369 energies of ionizing electrons used in this work, the ionization cross
370 sections at the electron energy used with the corresponding reference,
371 and the calibration method applied.

372 To convert the signal intensity I_i into the mole fraction X_i of the ith
373 species, electron-energy-dependent calibration factors (relative to
374 argon) $K_{i/Ar}$ were used:

$$K_{i/Ar} = \frac{I_i}{I_{Ar}} \frac{X_{Ar}}{X_i} \tag{1}$$

375

376 The mole fraction of argon at each height above the burner changed
377 only slightly due to the high dilution of the reactant gases, so it can be
378 assumed as nearly constant ($X_{Ar} = 0.8$). The calibration factors for the
379 reactants (H_2, CH_4, C_3H_8, O_2), the major products (CO, CO_2), and
380 some stable intermediates (acetylene, ethylene, ethane) were
381 determined by direct calibration experiments with gas mixtures of
382 known composition. These mixtures were preliminarily heated to 470
383 K to prevent argon clustering during molecular beam formation in the
384 probe. The signal intensity I_{Ar} was measured in all flame and
385 calibration experiments at the same electron energy (16.2 eV). It is
386 noteworthy that the calibration factors for the species did not depend
387 on pressure (at least, in the range from 1 to 5 atm). This indicates that
388 increasing the pressure does not influence the processes of molecular
389 beam formation and thus demonstrates the adequacy of our
390 experimental data provided in this paper. The calibration factor for
391 H_2O was evaluated using the H-balance equation and the signal
392 intensity of mass peak 18 in the postflame zone.

Table 2. Species Whose Mole Fractions Were Measured in the Flames[a]

m/z	formula	species name	IE (eV)	$\sigma(E)$ (Å²)	E (eV)	calibration
1	H	hydrogen atom	13.6	0.13[35]	16.65	RICS vs H_2
2	H_2	hydrogen	15.43	0.157[35]	18	direct
15	CH_3	methyl radical	9.84	0.241[35]	13.2	RICS vs CH_4
16	CH_4	methane	12.71	0.018[35]	14.35	direct
17	OH	hydroxyl	13.02	0.2, EST[36]	16.65	RICS vs H_2O
18	H_2O	water	12.62	0.143[35]	15.4	H material balance
26	C_2H_2	acetylene	11.41	0.182[35]	12.3	direct
28	C_2H_4	ethylene	10.53	0.237[35]	12.3	direct
28	CO	carbon monoxide	14.01	0.069[35]	15.4	direct
30	C_2H_6	ethane	11.52	0.126[35]	12.3	RICS vs C_2H_4
30	H_2CO	formaldehyde	10.88	0.053[35]	11.5	RICS vs C_2H_6
32	O_2	oxygen	12.07	0.102[35]	14.35	direct
40	Ar	argon	15.76		16.2	direct
40	C_3H_4	allene	10.22	0.816[35]	13.2	RICS vs CO_2, not separated
		propyne	10.48	0.685[35]	13.2	RICS vs CO_2, not separated
42	C_3H_6	propene	9.74	0.351[35]	12.3	RICS vs CO_2, not separated
42	C_2H_2O	ketene	9.617	0.24, EST[37]	12.3	RICS vs CO_2, not separated
44	C_3H_8	propane	10.94	0.154[35]	12.3	direct
44	CO_2	carbon dioxide	13.77	0.13[35]	15.4	direct

[a]IE, ionization energy (reference data); $\sigma(E)$, electron ionization cross section at the electron energy E and reference (EST, $\sigma(E)$ was estimated); RICS, relative ionization cross-section method.

393   The calibration factors for the other species, including H, OH, and
394 CH_3 radicals, were determined by the relative ionization cross section
395 (RICS) method proposed in ref 38. The same procedure has been
396 used and described in detail in our previous papers, for example, in ref
397 39. This method is based on the fact that the calibration factor $K_{i/Ar}$ is
398 proportional to the ionization cross section $\sigma_i(E)$ at the electron
399 energy E. Thus, the unknown calibration factor of an intermediate
400 species in the flame is related to the known calibration factor for the
401 stable species nearest in mass as follows: $K_{i/Ar} = K_{S/Ar}[\sigma_i(E_i)/\sigma_S(E_S)]$,
402 where the subscript i corresponds to the intermediate species, and the
403 subscript "S" corresponds to the nearest species with the known
404 calibration factor. The values of the ionization cross sections at a given
405 electron energy were taken from the NIST Electron-Impact Cross
406 Sections for Ionization and Excitation Database.[36]
407   The ionization cross sections of OH and ketene at the energies
408 indicated in Table 2 were estimated from their ionization cross
409 sections at 70 eV. The ratio of the ionization cross sections of two
410 different species at an electron energy differing from the ionization
411 potential by the same amount is known to be very close to the ratio of
412 the ionization cross sections of these species at an energy of 70 eV.
413 Thus, knowing the ionization cross section of ketene at 70 eV and the
414 dependence of the ionization cross section of a reference species (for
415 example, propene) on the energy of ionizing electrons, we can evaluate
416 the ionization cross section of ketene for lower energy. The ionization
417 cross section of ketene at 70 eV was evaluated using the method
418 proposed in ref 37. For OH, the ionization cross section at 70 eV was
419 taken from ref 36, and H_2O was used as a reference species.
420   As can be seen from Table 2, the species corresponding to mass
421 peaks 40 (allene + propyne) and 42 (propene + ketene) were not
422 separated due to very low difference between the ionization potentials
423 of the respective species. The calibration factor in this case was
424 calculated as the average value of the calibration factors of individual
425 species.
426   Typical statistical and relative uncertainties of MBMS signals are
427 below 20%[33] as the standard deviation for poor signal-to-noise ratios is
428 around 20%. Therefore, a relative comparison of each species from
429 different measurements and at different pressures offers good
430 precision. The resultant accuracy of determining the mole fraction
431 of the reactants and major stable products (O_2, H_2, CH_4, C_3H_8, CO_2,
432 H_2O, CO, C_2H_4, C_2H_2) was, as a rule, $\pm 20\%$ of the maximum value of
433 their mole fractions in the flame. For the other species, the mole
434 fractions were determined within a factor of about 2. The uncertainties
435 indicated above are mostly related to the calibration errors and the
436 inaccuracies of the ionization cross sections used.
437   Flame temperature profiles were measured by a Pt/Pt + 10% Rh
438 thermocouple located ∼0.05 mm from the tip of the sampling probe in
439 high-pressure flames and 0.2 mm from the probe tip in atmospheric-
440 pressure flames. The location of the thermocouple relative to the
441 probe tip and the burner during the experiments at 1, 3, and 5 atm was
442 controlled using a cathetometer. The thermocouple was manufactured
443 from a wire with a diameter of 0.02 mm. To prevent catalytic effects on
444 the thermocouple's surface, it was coated with a thin layer of SiO_2. The
445 resulting thermocouple had a diameter of 0.03 mm. The length of the
446 thermocouple shoulders was 8 mm (4 mm each). The length-to-
447 diameter ratio of the thermocouple was therefore >100, so the heat
448 losses into the cold ends of the thermocouple may be neglected. The
449 mounting unit of the thermocouple was similar to that described in
450 detail in our previous work.[40] The temperature values measured with
451 the thermocouple were corrected for radiative heat losses as described
452 in refs 41 and 42. The measurements of the temperature profiles were
453 repeated several times. The maximum scatter of the measured
454 temperatures in the postflame zone of all flames did not exceed ± 40
455 K. Nearly the same scatter of the measured values was in the zone of
456 the temperature gradient in the flame at 1 atm. However, when
457 temperature gradients were high enough, which was observed in the
458 flames at 3 and 5 atm, the scatter of the measured values was as great
459 as ± 150 K.
460   To correct the experimental profiles of the species' mole fractions
461 for the gas dynamic perturbations caused by the probe in flames, we
462 shifted them upstream to the burner by several probe orifice diameters.

463 We used the same method as in our previous studies.[32,33] All the
464 species mole fraction profiles of each flame were shifted by the same
465 distance. This distance was chosen so that the lowest height above the
466 burner at which the water mole fraction reached a maximum was the
467 same as that at which the maximum temperature was reached. In
468 particular, for our flame conditions, the shift of the profiles was 0.3,
469 0.02, and 0.06 mm at 1, 3, and 5 atm, respectively.

■ COMPUTER SIMULATION

470 The flame structure was simulated using the PREMIX[43] code
471 from the CHEMKIN II software package.[44] To take into
472 account the probe cooling effect on the flame, the calculations
473 were performed with measured temperature profiles as input
474 data using the TGIV keyword. The calculations were made
475 using the temperature profiles measured experimentally in the
476 flames perturbed by the probe. Thus, the energy conservation
477 equation has not been solved.
478   The profiles of the net rates of production of individual flame
479 species were calculated using the KINALC software,[45] which is
480 a postprocessor of the output files of the PREMIX code from
481 the CHEMKIN II software package. For the KINALC software
482 to be applied, the mechanism should consist only of irreversible
483 reactions; i.e., the original mechanism was primarily trans-
484 formed into irreversible reactions using the MECHMOD
485 software.[46] It is to be remembered that, despite the use of
486 irreversible reactions in the postprocessing, the resulting rates
487 of production for reversible reactions are provided in the paper.
488 In the simulation, four most recently developed mechanisms for
489 the oxidation of small hydrocarbons were used. Table 3
490 contains summary information on these mechanisms, including
491 the number of reactions and species, and the year of
492 publication.

Table 3. Reaction Mechanisms Used for Modeling the Flame Structure

mechanism	no. species	no. reactions	year	ref
AramcoMech 1.3	253	1542	2013	47
AramcoMech 2.0	493	2716	2016	48
Marinov et al.	155	689	1998	49
USC Mech II	111	784	2007	50

■ RESULTS AND DISCUSSION

494 Figure 1 shows the measured temperature profiles in the
495 burner-stabilized flames of $H_2/CH_4/C_3H_8$ fuel mixtures at
496 pressures of 1, 3, and 5 atm. As seen, the temperatures in the
497 postflame zone at 3 and 5 atm are rather close and are ∼280−
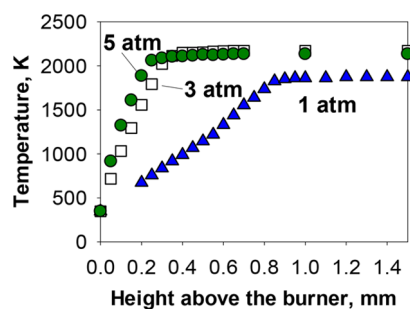
Figure 1. Measured temperature profiles in premixed laminar
stoichiometric $H_2/CH_4/C_3H_8/O_2/Ar$ flames stabilized on flat burners
at 1, 3, and 5 atm.
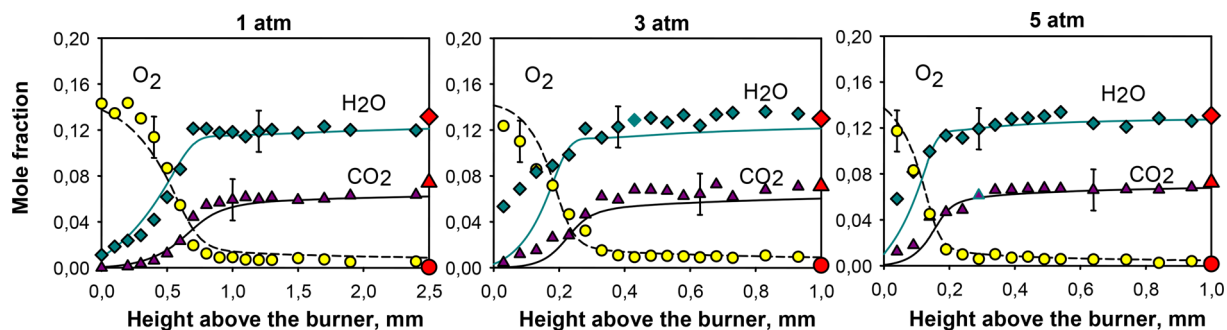
Figure 2. Measured and simulated profiles of mole fraction of oxygen and major products in $H_2/CH_4/C_3H_8$ flames at 1, 3, and 5 atm. Symbols, experimental data; curves, modeling using the AramcoMech 2.0 mechanism. Red symbols in the right parts of the plots correspond to the equilibrium mole fractions of the respective species.
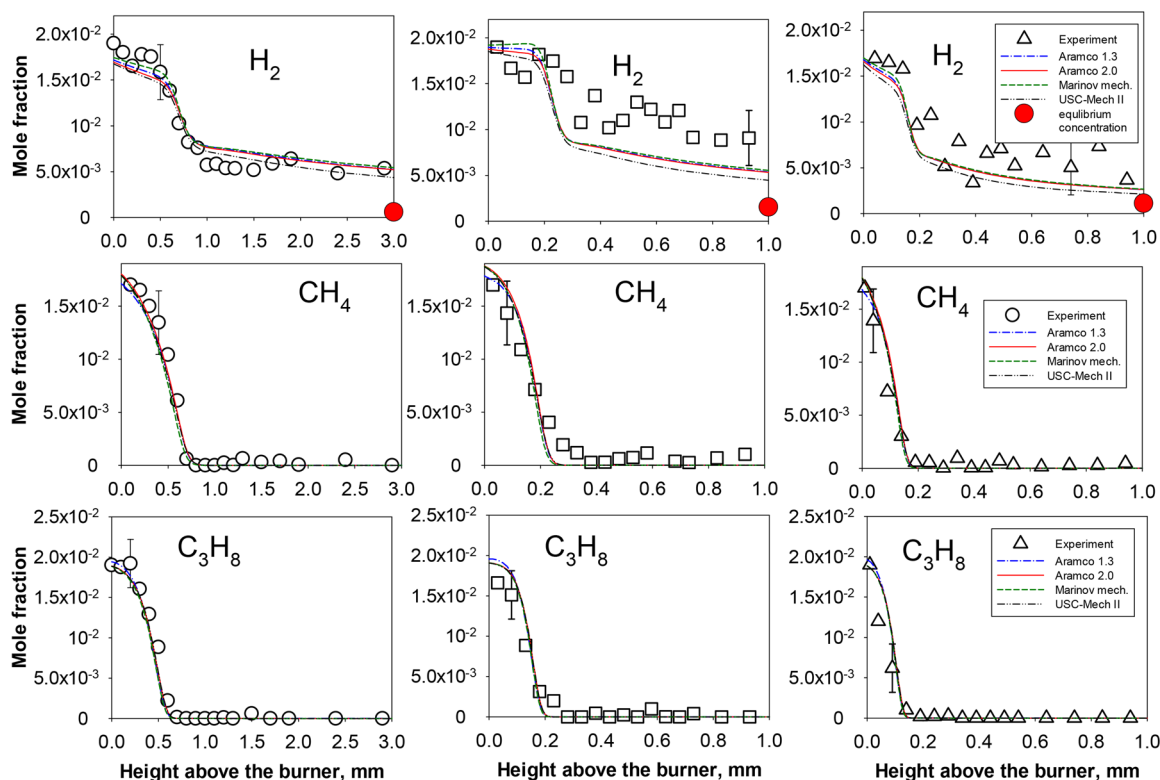
Figure 3. Mole fraction profiles of fuels in stoichiometric $H_2/CH_4/C_3H_8/O_2/Ar$ flames at pressures of 1 (left), 3 (middle), and 5 atm (right). Symbols, experiment; curves, simulation using different chemical kinetic mechanisms. The large red symbols in the right parts of the plots correspond to the thermodynamic equilibrium mole fractions of H_2.

300 K higher than the temperature at 1 atm. As the pressure grows, the width of the reaction zone decreases to ∼0.85, ∼0.35, and ∼0.25 mm at 1, 3, and 5 atm, respectively. Figure 2 contains the measured mole fraction profiles of oxygen and the primary combustion products (CO_2, H_2O), compared to the results of calculations using the AramcoMech 2.0 mechanism. The calculations were performed using three other kinetic mechanisms, and for all the species indicated above, all the mechanisms provided very close predictions of mole fraction profiles; thus, in Figure 2 we show only the numerical results obtained using AramcoMech 2.0. As seen from Figure 2, the experimental data are in good agreement with the modeling results. It can also be seen that in the postflame zone (at distances of 2.5, 1, and 1 mm from the burner at 1, 3, and 5 atm, respectively), the measured and calculated mole fractions of O_2, CO_2, and H_2O coincide, within the measurement error

limits, with the calculated thermodynamic equilibrium mole fractions.

To analyze the mutual influence of the parent fuels on the kinetics of their oxidation, we compared the measured and calculated mole fraction profiles of the fuels at different pressures (Figure 3). It can be seen from Figure 3 that hydrogen is not fully consumed in all the flames; therefore, it is difficult to determine the width of its consumption zone. In any case, it is greater than the consumption zone of methane. It can also be seen that the consumption zone of propane is even smaller than the consumption zone of methane. The observed trend persists when the pressure is increased. In addition, it should be pointed out that both the measured and calculated mole fraction profiles of hydrogen have a characteristic kink near the burner surface (at distances of 0.6, 0.2, and 0.15 mm at 1, 3, and 5 atm, respectively), and the mole fraction profiles of

F
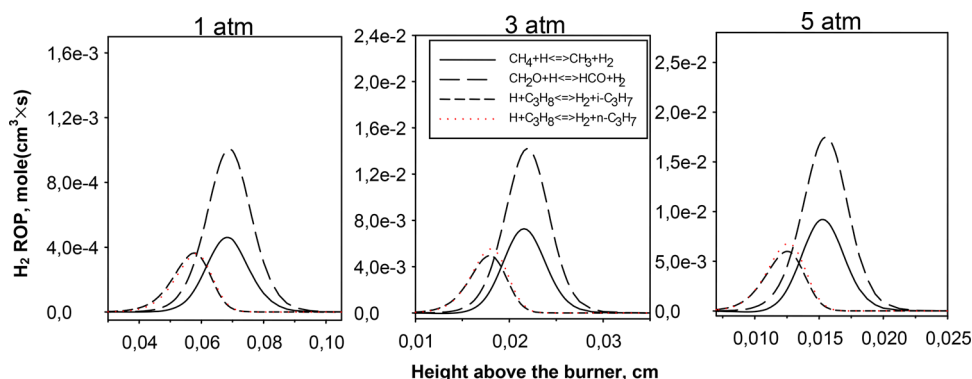
Figure 4. Profiles of rates of hydrogen production (H$_2$ ROP) in individual reactions in H$_2$/CH$_4$/C$_3$H$_8$/O$_2$/Ar flames at 1, 3, and 5 atm (AramcoMech 2.0).
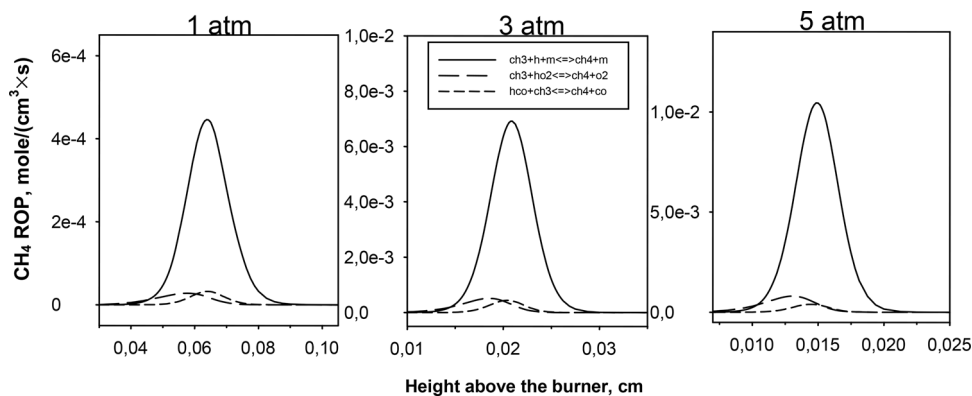
Figure 5. Profiles of rates of methane production (CH$_4$ ROP) in individual reactions in H$_2$/CH$_4$/C$_3$H$_8$/O$_2$/Ar flames at 1, 3, and 5 atm (AramcoMech 2.0).

CH$_4$ and C$_3$H$_8$ do not have it. It is evident that this shape of the H$_2$ profile is related to the simultaneous processes of its production and consumption in the reaction zone of the flame. It is noteworthy that different widths of the consumption zones of fuel components were also observed by De Ferrieres et al.[29,30] in a flame of natural gas and hydrogen (40%/60%): the consumption zone of H$_2$ was greater than those of C$_3$H$_8$ and CH$_4$. It can also be seen from Figure 3 that, at pressures of 1 and 3 atm, the measured and calculated mole fractions of hydrogen at distances of 3 and 1 mm from the burner surface, respectively, are much higher than its equilibrium mole fraction. As the pressure rises to 5 atm, this divergence decreases considerably.

To explain the large width of the hydrogen consumption zone in the H$_2$/CH$_4$/C$_3$H$_8$ flames, we analyzed the main reaction pathways of its production at 1, 3, and 5 atm. Figure 4 shows the profiles of the rates of hydrogen production (H$_2$ ROP) in the reactions making the major positive contribution to the total rate of hydrogen production near the burner surface at 1, 3, and 5 atm. The key pathways of hydrogen production are the interactions between hydrogen atoms and form-aldehyde, methane, and propane molecules. Reaction R1 makes the major contribution to the total rate of hydrogen production:

$$CH_2O + H \leftrightarrow HCO + H_2 \tag{R1}$$
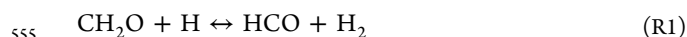
The second in importance is the reaction of the H atom with methane:

$$CH_4 + H \leftrightarrow CH_3 + H_2 \tag{R2}$$
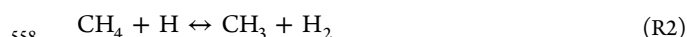
The reactions between H and the propane molecule producing propyl and isopropyl radicals (reactions R3 and R4) yield somewhat smaller values of H$_2$ ROP. The profiles of H$_2$ ROP for these stages are located somewhat closer to the burner surface compared to the profiles of reactions R1 and R2.

$$C_3H_8 + H \leftrightarrow H_2 + n\text{-}C_3H_7 \tag{R3}$$

$$C_3H_8 + H \leftrightarrow H_2 + i\text{-}C_3H_7 \tag{R4}$$

Although the absolute rates of reactions R1−R4 increased with pressure, their relative contributions to H$_2$ formation practically did not change (Figure 4). Thus, the greater width of the consumption zone of hydrogen in the H$_2$/CH$_4$/C$_3$H$_8$/O$_2$/Ar flame, compared to those of propane and methane, results from the production of hydrogen in the reactions of H atoms with formaldehyde, methane, and propane. Consumption of molecular hydrogen occurs in the flames via the reactions of chain branching H$_2$ + O ↔ H + OH and chain propagation H$_2$ + OH ↔ H + H$_2$O.

A similar analysis was carried out for methane, for which the consumption zone width in the flame is, as mentioned above, somewhat higher than that of propane. Figure 5 shows the profiles of the rates of methane production (CH$_4$ ROP) in the reactions making the major positive contribution to the total rate of methane production. It can be seen that the recombination of methyl radical and hydrogen atom (reaction R5) plays the crucial role in methane production in the flame.

$$CH_3 + H + M \leftrightarrow CH_4 + M \tag{R5}$$

G
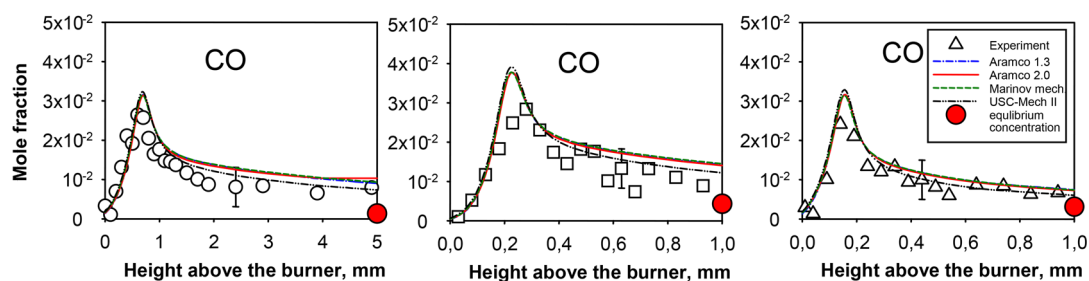
Figure 6. CO mole fraction profiles in stoichiometric $H_2/CH_4/C_3H_8/O_2/Ar$ flames at pressures of 1 (left), 3 (middle), and 5 atm (right). Symbols, experiment; curves, modeling using different chemical kinetics mechanisms. The large red symbols in the right parts of the plots correspond to the thermodynamic equilibrium mole fractions of CO.
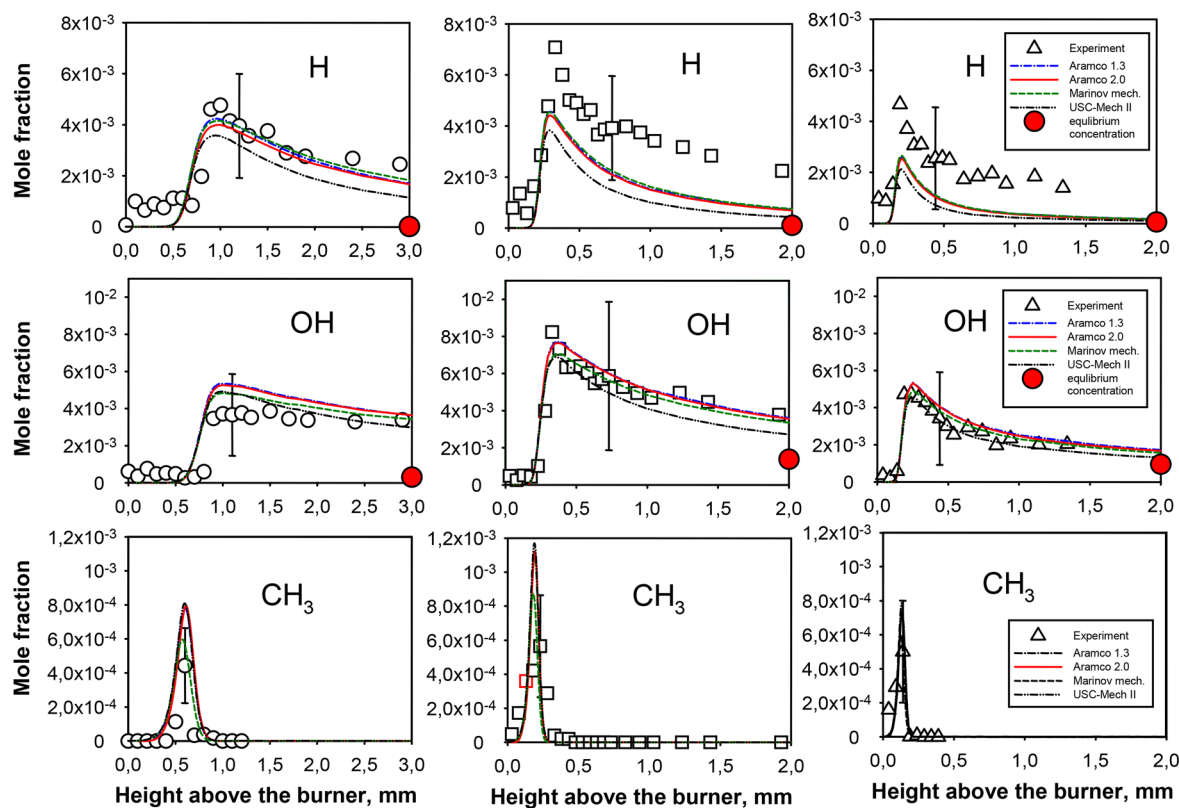
Figure 7. Mole fraction profiles of H, OH, and CH_3 radicals in stoichiometric $H_2/CH_4/C_3H_8/O_2/Ar$ flames at pressures of 1 (left), 3 (middle), and 5 atm (right). Symbols, experiment; curves, simulation using different chemical kinetics mechanisms. The large red symbols in the right parts of the plots correspond to the equilibrium mole fractions of the respective species.

The contribution of the other reactions to the production of methane is negligibly small. Reactions R2 and R5 form a cycle of methane consumption to produce a methyl radical, which is later transformed into methane: $CH_4 \leftrightarrow CH_3$. Both reactions proceed with the H consumption and hydrogen and/or methane production. It is also worth noting (Figure 5) that the relative contributions of the above reactions of methane production practically do not change with pressure.

The above arguments explain the observed delay in the consumption of hydrogen and methane in the flame. However, it is not clear why propane is consumed faster than methane: reactions similar to reaction R5 with similar kinetic parameters are present in the mechanism, for example, $n\text{-}C_3H_7 + H \leftrightarrow C_3H_8$, $i\text{-}C_3H_7 + H \leftrightarrow C_3H_8$, as well as some others, which should also impede the consumption of propane near the burner surface; however, this was not observed in the experiment or in simulation.

To explain this fact, the reaction pathways of methane and propane consumption included in the AramcoMech 2.0 mechanism were analyzed in all flames. Comparison shows that the number of the pathways of methane consumption differs significantly from that of propane consumption. Methane is consumed in five different reactions, while propane consumption occurs in 33 steps. It is likely that the processes of propane production in recombination of n-propyl or isopropyl radicals with hydrogen atoms occur, but their rates are small compared to the total rate of propane consumption, and they cannot significantly influence the shape of the mole fraction profile of propane in the flame.

Figure 6 shows the measured and calculated mole fraction profiles of CO. As can be seen, all mechanisms predict well the experimental data; moreover, the predictions given by the mechanisms are very similar. It can be seen that, as the pressure increases from 3 to 5 atm, both the peak and postflame CO
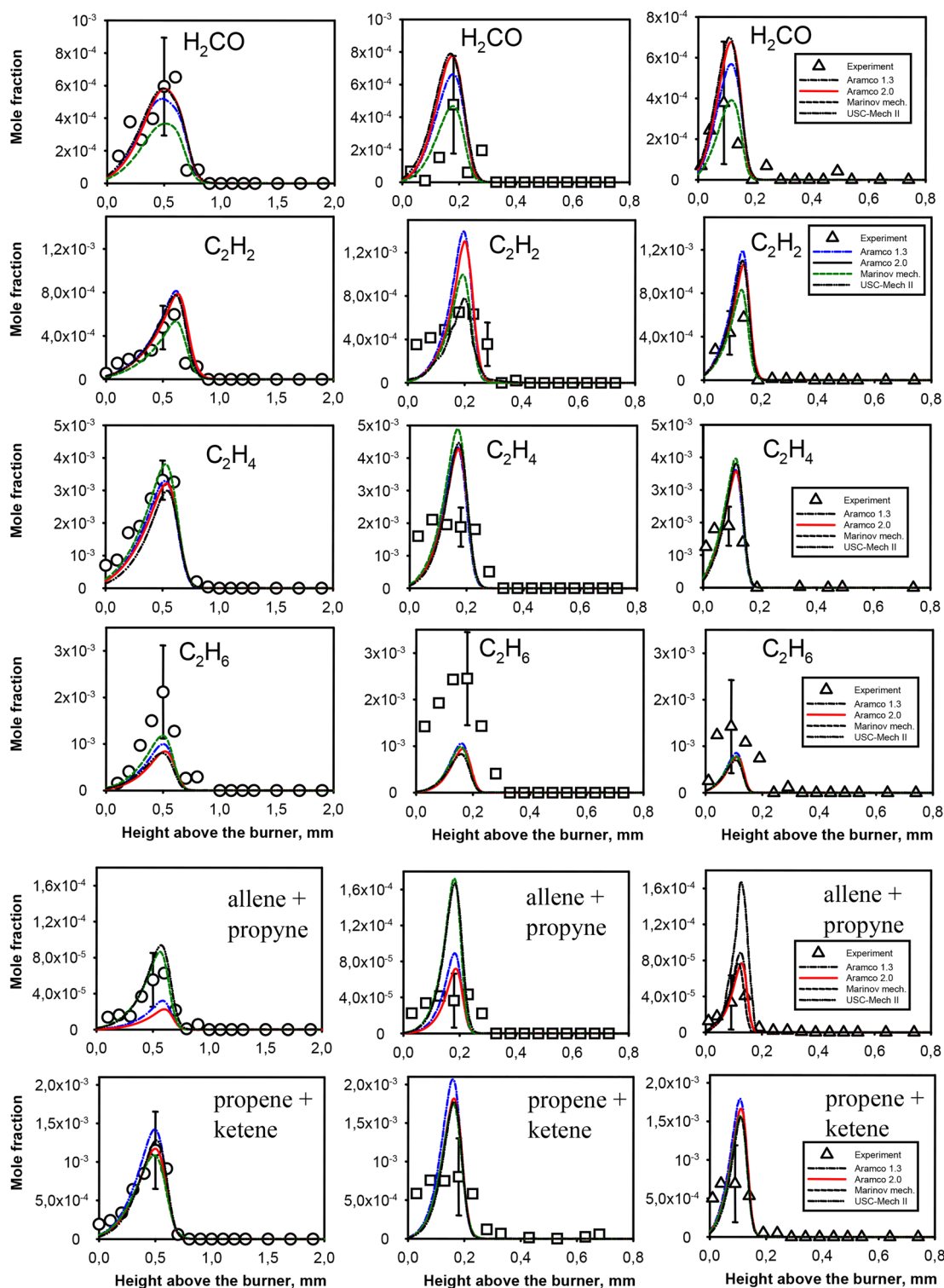
Figure 8. Mole fraction profiles of formaldehyde, acetylene, ethylene, ethane, and C_3H_4 (allene + propyne) and $C_3H_6 + C_2H_2O$ (propene + ketene) in stoichiometric $H_2/CH_4/C_3H_8/O_2/Ar$ flames at pressures of 1 (left), 3 (middle), and 5 atm (right). Symbols, experiment; curves, simulation using different chemical kinetics mechanisms.

mole fractions slightly decrease. As the postflame temperatures of these flames are similar, we can speak of an increase in the completeness of combustion as the pressure rises. This is also seen from a comparison of the measured and equilibrium mole fractions of CO in the postflame zone of the flames: at a pressure of 5 atm, the postflame mole fraction of CO is close to its equilibrium mole fraction.

Figure 7 demonstrates the mole fraction profiles of H, OH, and CH_3 radicals in the $H_2/CH_4/C_3H_8/O_2/Ar$ flame at 1, 3, and 5 atm. As seen, the rise of pressure insignificantly affects the peak mole fractions of the radicals in the flames, although they were expected to decrease with pressure, as was demonstrated previously in hydrogen[32] and methane[33] flames.
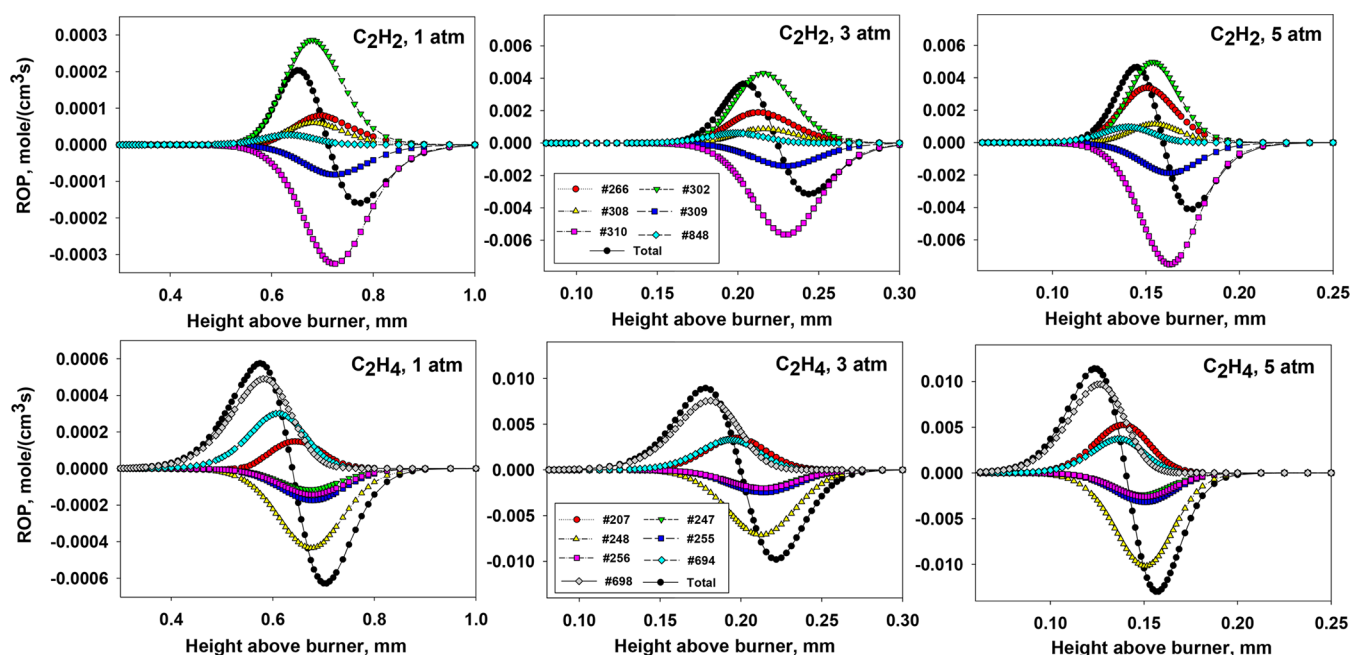
Figure 9. Profiles of rates of production (ROP) of acetylene and ethylene in the crucial reactions in the flame of $H_2/CH_4/C_3H_8/O_2/Ar$ at 1, 3, and 5 atm (AramcoMech 2.0). The reaction numbers as they appear in AramcoMech 2.0 are indicated in the legends. Curves with black circles: total rates of production of acetylene (top) and ethylene (bottom). The reactions corresponding to the numbers provided are listed in Table 4 (for acetylene) and Table 5 (for ethylene). The production rate profiles for reactions having contributions less than 5% are not shown.

The mole fractions of the major flame radicals are known to depend significantly on the flame temperature.

Earlier[32,33] we were able to determine their decrease with increasing pressure because, under those flame conditions, the flame temperature remained practically constant at all pressures. Unfortunately, we could not find conditions for $H_2/CH_4/C_3H_8$ flames under which their postflame temperatures would be equal at different pressures (Figure 1). Therefore, the trend of reduction in the peak mole fraction of radicals with pressure is seen in Figure 7 only when the pressure changes from 3 to 5 atm, as under these conditions the postflame temperatures practically did not differ (Figure 1). It can also be noted that, as the pressure rises, the measured and calculated mole fractions of H and OH radicals in the postflame zone (at a distance of 2−3 mm from the burner surface) approach the equilibrium values.

Analysis of the employed chemical kinetic mechanisms has shown that the reduction in the mole fraction of H radicals is primarily related to the reaction H + O$_2$ (+M) ↔ HO$_2$ (+M), the contribution of which to the consumption of H atoms increases with a rise in pressure. As the H mole fraction also largely determines the concentration of hydroxyl, mostly due to the reaction H + O$_2$ ↔ O + OH, the mole fraction of OH also decreases. In a similar way, the mole fraction of CH$_3$ decreases due to an increase in the contribution of the reaction CH$_3$ + H + M ↔ CH$_4$ + M to its consumption with increasing pressure.

Figure 8 shows the measured and simulated mole fraction profiles of formaldehyde, primary C$_2$ hydrocarbons, and the species whose contributions to the respective mass peaks were not separated (allene + propyne and propene + ketene). As is seen, all the mechanisms similarly predict the mole fraction profiles of most of these species in flame, except for formaldehyde and C$_3$H$_4$ (allene + propyne). At 1 atm, all the models well predict the peak mole fractions of the intermediates. However, at pressures of 3 and 5 atm, the calculated peak mole fractions are 1.5−2 times larger than the experimental values for all the species except for C$_2$H$_6$. The measurements demonstrated that increasing the pressure from 1 to 5 atm insignificantly affected the peak mole fractions of these intermediates: for all the species, except for C$_2$H$_6$, the peak mole fractions are reduced by a factor of 1.3−1.5. However, the results of simulation show the opposite trend for these species: a 1.2−1.8-fold increase in their peak mole fractions. For C$_2$H$_6$, the models underpredict the measured peak mole fractions by about a factor of 2−2.5. In addition, the calculated peak mole fraction of C$_2$H$_6$ practically does not change with pressure, whereas, according to measurements, it does not change only in the pressure range from 1 to 3 atm; as the pressure is further increased from 3 to 5 atm, it is reduced by a factor of ∼1.7.

Thus, all the mechanisms used satisfactorily reproduce the experimentally observed tendency of the peak mole fractions of H$_2$CO, C$_2$H$_2$, C$_2$H$_4$, allene + propyne, and propene + ketene to decrease with a rise in pressure from 3 to 5 atm. However, all the mechanisms predict an increase in the peak mole fractions of these species as the pressure rises from 1 to 3 atm, which is not observed experimentally. Note that a similar result was obtained in our previous study, in which, in addition to other issues, the effect of the pressure change within the same limits on the peak mole fractions of ethylene and acetylene in methane flames was investigated.[33] It was found in that study that, as the pressure rose from 1 to 3 atm, the mechanisms used (AramcoMech 1.3 and GRI-Mech 3.0) predicted an increase in the peak mole fractions of C$_2$H$_2$ and C$_2$H$_4$, whereas we observed their reduction in the experiment. Analysis of the reaction pathways allowed us to state that this disagreement is related to the fact that those models do not adequately predict the pressure-dependent chemistry of acetylene and ethylene production and need to be improved.

In this study, we also analyzed the pathways of production and consumption of acetylene and ethylene for the AramcoMech 2.0 mechanism. Figure 9 shows the profiles of the rates of production and consumption of acetylene and ethylene in the key reactions in $H_2/CH_4/C_3H_8$ flames at different pressures. It is seen from the plots in Figure 9 that active production and consumption of ethylene in flame occur slightly closer to the burner than those of acetylene. In addition, it is to be noted that the maximum total rates of production of C_2H_2 and C_2H_4 increase by factors of ~20 and ~16 with a pressure rise from 1 to 3 atm, respectively, but with a further pressure increase to 5 atm, they change only slightly. However, the total rates of consumption of these species also increase with pressure, so that the mole fractions of acetylene and ethylene in the flame eventually do not change so significantly with pressure (Figure 8).

The reaction numbers of which are provided in the legends for the plots in Figure 9 are listed in Tables 4 and 5. In order to

Table 4. Reactions Providing the Largest Contribution to the Total Rate of Acetylene Production (AramcoMech 2.0) and Their Integrated Contributions (%) to the Production (+) and Consumption (−) of Acetylene at 1, 3, and 5 atm

reaction no.	reaction	contribution to total C_2H_2 production (consumption) (%)		
		1 atm	3 atm	5 atm
302	$C_2H_3 + H \leftrightarrow C_2H_2 + H_2$	56.78	48.31	40.97
266	$C_2H_2 + H (+M) \leftrightarrow C_2H_3 (+M)$	15.01	23.30	31.05
308	$C_2H_2 (+M) \leftrightarrow H_2CC (+M)$	11.74	9.67	9.31
848	$CH_3 + C_2H_2 \leftrightarrow C_3H_5$	5.23	7.25	8.51
309	$C_2H_2 + O \leftrightarrow CH_2 + CO$	−19.10	−19.10	−18.63
310	$C_2H_2 + O \leftrightarrow HCCO + H$	−76.38	−76.37	−74.52

numerically evaluate the contribution of each reaction to the total rate of production of acetylene or ethylene, we calculated the integrated rates of all reactions involving acetylene and ethylene in the flame (ω_i) in the same way as was done previously:[34]

$$\omega_i = \int_0^\infty \omega_i'\, dt = \int_0^\infty \frac{\omega_i'}{\nu}\, dx \qquad (2)$$

where ω_i' is the local rate of the ith reaction, mol/(cm^3·s), ν is the local gas velocity (cm/s), and x is the distance from the burner (integration was carried out over the entire flame zone). The obtained values of ω_i were normalized by the sum of integrated production or consumption rates of acetylene and

ethylene in all the reactions. Thus, we obtained the contributions of the reactions to the production or consumption of acetylene and ethylene. These values (in percent) are given in Tables 4 and 5.

As seen from Figure 9, the reaction of the vinyl radical with the hydrogen atom is the main pathway for acetylene production in the flames: $C_2H_3 + H \leftrightarrow C_2H_2 + H_2$ (reaction 302). In addition, acetylene is produced from vinyl by the reaction $C_2H_3 (+M) \leftrightarrow C_2H_2 + H (+M)$ (reaction R266, which is the reverse of reaction 266) and by the reaction of vinylidene isomerization with third-body participation $H_2CC (+M) \leftrightarrow C_2H_2 (+M)$ (reaction R308). Acetylene is also produced by the allyl decomposition reaction $C_3H_5-S \leftrightarrow CH_3 + C_2H_2$ (reaction R848). Notice that the maximum of the rate of this reaction is slightly shifted to the burner compared to those of other reactions. Acetylene consumption mostly proceeds in its reactions with the oxygen atom (reactions 309 and 310), and their contribution does not change with pressure.

Reactions 266 and 308 in the AramcoMech 2.0 mechanism have rate constants which depend on pressure. As seen from Table 4, the integrated contribution of reaction 266 to the production of acetylene increases more than 2-fold (from ~15 to ~31%) as the pressure increases from 1 to 5 atm. This may be the reason for the decrease in the contribution of the main reaction of its production (reaction R302) as the pressure increases (from ~57 to ~41%). The fact that the model and the experiment give opposite trends for the peak mole fraction of acetylene with pressure in the range from 1 to 3 atm indicates a need to thoroughly investigate pressure dependence of the rate constant of the reaction $C_2H_3 (+M) \leftrightarrow C_2H_2 + H (+M)$. This, however, is beyond the scope of the present study.

Ethylene is produced in the reactions of monomolecular decomposition of the n-propyl radical n-$C_3H_7 \leftrightarrow C_2H_4 + CH_3$ (reaction R698), decomposition of the ethyl radical $C_2H_5 (+M) \leftrightarrow C_2H_4 + H (+M)$ (reaction R207), and interaction between propylene and the hydrogen atom $C_3H_6 + H \leftrightarrow C_2H_4 + CH_3$ (reaction 694). Its consumption mainly proceeds in reactions with H, O, and OH (Figure 9 and Table 5). As is seen from Table 5, just as in the case with acetylene, the contribution of different reactions to the total integrated rate of ethylene consumption does not change with pressure. Among the three above-mentioned reactions of ethylene production, reaction 207 has a pressure-dependent rate constant, so its contribution to the total integrated rate of ethylene production increases with pressure. When the pressure increases from 1 to 3 atm, this contribution is nearly doubled (from 10.85 to 21.06%), and with a further pressure rise, it increases to approximately 25%. It seems likely that the pressure dependence of the rate constant of this reaction should be revised in order to obtain

Table 5. Reactions Providing the Largest Contribution to the Total Rate of Ethylene Production (AramcoMech 2.0) and Their Integrated Contributions (%) to Production (+) and Consumption (−) of Ethylene at 1, 3, and 5 atm

reaction no.	reaction	contribution to total C_2H_4 production (consumption) (%)		
		1 atm	3 atm	5 atm
698	$C_2H_4 + CH_3 \leftrightarrow n$-$C_3H_7$	54.44	53.70	51.88
207	$C_2H_4 + H (+M) \leftrightarrow C_2H_5 (+M)$	10.85	21.06	25.51
694	$C_3H_6 + H \leftrightarrow C_2H_4 + CH_3$	29.61	20.42	17.59
247	$C_2H_4 + H \leftrightarrow C_2H_3 + H_2$	−12.39	−13.87	−12.35
256	$C_2H_4 + O \leftrightarrow CH_2CHO + H$	−16.00	−14.57	−13.92
255	$C_2H_4 + O \leftrightarrow CH_3 + HCO$	−19.56	−17.81	−17.02
248	$C_2H_4 + OH \leftrightarrow C_2H_3 + H_2O$	−50.14	−51.65	−54.46
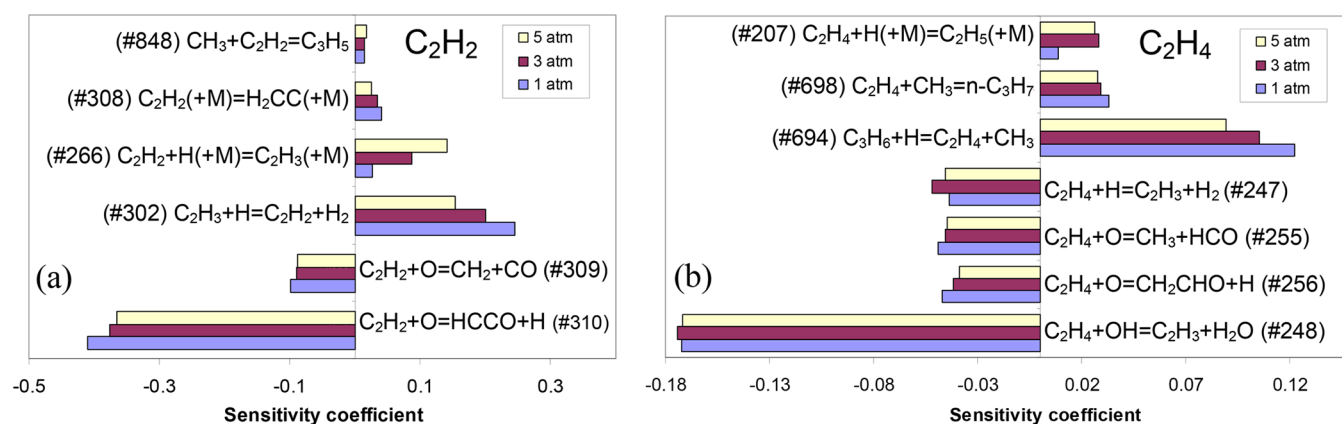
Figure 10. Sensitivity coefficients of acetylene (a) and ethylene (b) in $H_2/CH_4/C_3H_8/O_2/Ar$ flames at 1, 3, and 5 atm. The sensitivity coefficients are calculated for the heights above the burner corresponding to the maximum mole fractions of C_2H_2 and C_2H_4, respectively.

reasonable agreement between the experiment and the model for the pressure influence on the peak mole fraction of ethylene in the flame.

Although the production/consumption rates can be used to identify the reaction pathways related to the species of interest, they do not necessarily reflect the correlation between the rate parameters and the simulated profiles. Thus, a sensitivity analysis was also performed to make reasonable suggestions for updating the mechanisms. The sensitivity coefficients of C_2H_2 and C_2H_4 were calculated for the whole range of heights above the burner. However, a comparison of the sensitivity coefficients of the selected species at different pressures is reasonable only for the heights above the burner where these species reach maximum mole fractions. Parts a and b of Figure 10 show the sensitivity coefficients of C_2H_2 and C_2H_4, respectively, at the heights above the burner corresponding to the maximum mole fractions of these species. The C_2H_2 sensitivities were calculated at 0.63, 0.2, and 0.13 mm from the burner at 1, 3, and 5 atm, respectively. The sensitivities of C_2H_4 were calculated at 0.54, 0.17, and 0.11 mm from the burner at 1, 3, and 5 atm, respectively.

The most sensitive reactions only are shown in Figure 10. It is interesting to note that all these reactions were mentioned above as the reactions playing a key role in the formation/consumption of acetylene and ethylene. As is seen from the diagrams in Figure 10, the formation of acetylene and the formation of ethylene are very sensitive to the rate constants of reactions 310 and 248, respectively. These reactions, as shown above (see Tables 4 and 5), play a crucial role in the consumption of these species. Reactions 302 and 694 also exhibit high sensitivity coefficients. However, it is noteworthy that the pressure change in the range from 1 to 5 atm results in a notable increase in the sensitivity coefficients of the reactions $C_2H_2 + H\ (+M) \leftrightarrow C_2H_3\ (+M)$ (reaction 266) and $C_2H_4 + H\ (+M) \leftrightarrow C_2H_5\ (+M)$ (reaction 207) only. This implies that varying the rate constants of these reactions can have different effects on the calculated peak mole fractions of C_2H_2 and C_2H_4 at different pressures. While the sensitivity coefficients of reactions 302 and 694 slightly decrease with pressure, the sensitivities of other reactions remain virtually unchanged. Therefore, the sensitivity analysis also shows that revising the rate constants of reactions 266 and 207 can help in obtaining reasonable agreement between the experimental and model results for the pressure influence on the peak mole fractions of acetylene and ethylene in the flame.

CONCLUSION

Using the experimental method and numerical modeling, we studied the thermal and chemical structures of stoichiometric flames of blended fuel $H_2/CH_4/C_3H_8$ stabilized on a flat burner at atmospheric and elevated pressures. Molecular-beam mass spectrometry was employed to measure the mole fraction profiles of the initial components of the fuel mixture, the main combustion products, and intermediates, including the mole fraction profiles of H atoms and OH and CH_3 radicals.

Comparison of the experimental data with the results of numerical modeling has shown that all four mechanisms satisfactorily predict the distribution of the mole fractions of the initial reactants, the final combustion products, and most of the intermediate flame species. Agreement is observed at both atmospheric and elevated pressures. All the mechanisms used in modeling give close mole fractions of the flame species in spite of the different numbers of reactions and components and dates of issue. Moreover, for all the mechanisms, the differences between the modeling and experimental results were similar. This indicates that the authors developing new models focus mostly on the model extension, i.e., the addition of new species and reactions involving them (e.g., AramcoMech 2.0), rather than on the revision of the rate constants of "well-known" reactions and their pressure dependences. Clearly, this is due to the lack of reliable experimental data suitable for validating the mechanisms, but this problem has been pointed out.

The consumption zones of the fuel components have been established to be significantly different. Hydrogen (H_2) was shown to have the widest consumption zone in the flames, while C_3H_8 had the narrowest one. Analysis of the consumption rates of the fuel components has shown that this effect is related not only to the different reactivities of the fuel components, but also to the fact that the presence of methane and propane gives rise to additional pathways of hydrogen production, resulting in a significant expansion of the width of the H_2 consumption zone in flames. The pathways of methane production, including $CH_3 + H + M \leftrightarrow CH_4 + M$, $CH_3 + HO_2 \leftrightarrow CH_4 + O_2$, and $CH_3 + HCO \leftrightarrow CH_4 + CO$, play an important role in flames containing increased mole fractions of H and CH_3 radicals due to the presence of hydrogen and propane, respectively, in the unburnt gases.

At atmospheric pressure, all the mechanisms used satisfactorily predict the peak mole fractions for intermediate hydrocarbons (ethylene and acetylene) that play an important role in the formation of polycyclic aromatic hydrocarbons, as

well as for allene + propyne, propene + ketene, and formaldehyde. However, as the pressure is increased to 3 atm, the same mechanisms overpredict the peak mole fraction of all these species. The analysis of the pathways of production and consumption of C_2H_4 and C_2H_2 in the AramcoMech 2.0 mechanism[48] at atmospheric and elevated pressures revealed the key reactions responsible for these processes. The observed disagreement seems to be due to the incorrect pressure dependences of the rate constants of the reactions C_2H_5 (+M) $\leftrightarrow C_2H_4$ + H (+M) and C_2H_3 (+M) $\leftrightarrow C_2H_2$ + H (+M) used in these models, which therefore need to be refined. The experimental data obtained may be used for testing other kinetic mechanisms not mentioned in this paper that simulate the combustion of multicomponent fuel mixtures containing hydrogen, methane, and propane.

■ AUTHOR INFORMATION

Corresponding Author

*E-mail: knyazkov@kinetics.nsc.ru.

ORCID ⊙

D. A. Knyazkov: 0000-0002-6819-4935

Notes

The authors declare no competing financial interest.

■ ACKNOWLEDGMENTS

■ REFERENCES

(1) Kamada, T.; Nakamura, H.; Tezuka, T.; Hasegawa, S.; Maruta, K. *Combust. Flame* **2014**, *161*, 37−48.

(2) Baloo, M.; Dariani, B. M.; Akhlaghi, M.; AghaMirsalim, M. *Fuel* **2016**, *170*, 235−244.

(3) Petersen, E. L.; Kalitan, D. M.; Simmons, S.; Bourque, G.; Curran, H. J.; Simmie, J. M. *Proc. Combust. Inst.* **2007**, *31*, 447−454.

(4) Rogers, T.; Petersen, P.; Koopmans, L.; Lappas, P.; Boretti, A. *Int. J. Hydrogen Energy* **2015**, *40*, 1584−1597.

(5) Zhang, Y.; Huang, Z.; Wei, L.; Zhang, J.; Law, C. K. *Combust. Flame* **2012**, *159*, 918−931.

(6) Yu, G.; Law, C. K.; Wu, C. K. *Combust. Flame* **1986**, *63*, 339−347.

(7) Huang, Z.; Zhang, Y.; Zeng, K.; Liu, B.; Wang, Q.; Jiang, D. *Combust. Flame* **2006**, *146*, 302−311.

(8) Hu, E.; Huang, Z.; He, J.; Jin, C.; Zheng, J. *Int. J. Hydrogen Energy* **2009**, *34*, 4876−4888.

(9) Ilbas, M.; Crayford, A. P.; Yilmaz, I.; Bowen, P. J.; Syred, N. *Int. J. Hydrogen Energy* **2006**, *31*, 1768−1779.

(10) Coppens, F. H.V.; Konnov, A. A. *Fuel* **2008**, *87*, 2866−2870.

(11) Konnov, A. A.; Riemeijer, R.; de Goey, L. P. H. *Fuel* **2010**, *89*, 1392−1396.

(12) Coppens, F. H. V.; De Ruyck, J.; Konnov, A. A. *Exp. Therm. Fluid Sci.* **2007**, *31*, 437−444.

(13) Konnov, A. A.; Riemeijer, R.; Kornilov, V. N.; de Goey, L. P. H. *Exp. Therm. Fluid Sci.* **2013**, *47*, 213−223.

(14) Hermanns, R. T. E.; Konnov, A. A.; Bastiaans, R. J. M.; de Goey, L. P. H.; Lucka, K.; Kohne, H. *Fuel* **2010**, *89*, 114−121.

(15) Yu, J. F.; Yu, R.; Fan, X. Q.; Christensen, M.; Konnov, A. A.; Bai, X. S. *Combust. Flame* **2013**, *160*, 1276−1286.

(16) De Goey, L. P. H.; Van Maaren, A.; Quax, R. M. *Combust. Sci. Technol.* **1993**, *92*, 201−207.

(17) Van Maaren, A.; Thung, D. S.; de Goey, L. P. H. *Combust. Sci. Technol.* **1994**, *96*, 327−344.

(18) Di Sarli, V.; Di Benedetto, A. *Int. J. Hydrogen Energy* **2007**, *32*, 637−646.

(19) Chen, Z.; Dai, P.; Chen, S. *Int. J. Hydrogen Energy* **2012**, *37*, 10390−10396.

(20) Park, O.; Veloo, P. S.; Liu, N.; Egolfopoulos, F. N. *Proc. Combust. Inst.* **2011**, *33*, 887−894.

(21) Okafor, E. C.; Hayakawa, A.; Nagano, Y.; Kitagawa, T. *Int. J. Hydrogen Energy* **2014**, *39*, 2409−2417.

(22) Wu, F.; Kelley, A. P.; Tang, C.; Zhu, D.; Law, C. K. *Int. J. Hydrogen Energy* **2011**, *36*, 13171−13180.

(23) Vu, T. M.; Park, J.; Kim, J. S.; Kwon, O. B.; Yun, J. H.; Keel, S. I. *Int. J. Hydrogen Energy* **2011**, *36*, 6914−6924.

(24) Donohoe, N.; Heufer, A.; Metcalfe, W. K.; Curran, H. J.; Davis, M. L.; Mathieu, O.; Plichta, D.; Morones, A.; Petersen, E. L.; Güthe, F. *Combust. Flame* **2014**, *161*, 1432−1443.

(25) Halter, F.; Chauveau, C.; Djebaïli-Chaumeix, N.; Gökalp, I. *Proc. Combust. Inst.* **2005**, *30*, 201−208.

(26) Petersen, E. L.; Hall, J. M.; Smith, S. D.; de Vries, J.; Amadio, A. R.; Crofton, M. W. *J. Eng. Gas Turbines Power* **2007**, *129*, 937−944.

(27) Dagaut, P.; Nicolle, A. *Proc. Combust. Inst.* **2005**, *30*, 2631−2638.

(28) Dagaut, P.; Dayma, G. *Int. J. Hydrogen Energy* **2006**, *31*, 505−515.

(29) De Ferrieres, S.; Lefort, B.; Montero, M.; El Bakali, A.; Pauwels, J. F. *Combust. Flame* **2008**, *154*, 601−623.

(30) De Ferrieres, S.; El Bakali, A.; Gasnot, L.; Montero, M.; Pauwels, J. F. *Fuel* **2013**, *106*, 88−97.

(31) Mze Ahmed, A.; Mancarella, S.; Desgroux, P.; Gasnot, L.; Pauwels, J. F.; El Bakali, A. *Int. J. Hydrogen Energy* **2016**, *41*, 6929−6942.

(32) Knyazkov, D. A.; Dmitriev, A. M.; Bolshova, T. A.; Shvartsberg, V. M.; Shmakov, A. G.; Korobeinichev, O. P. *Proc. Combust. Inst.* **2017**, *36*, 1233−1240.

(33) Dmitriev, A. M.; Knyazkov, D. A.; Bolshova, T. A.; Tereshchenko, A. G.; Paletsky, A. A.; Shmakov, A. G.; Korobeinichev, O. P. *Combust. Flame* **2015**, *162*, 3946−3959.

(34) Botha, J. P.; Spalding, D. B. *Proc. R. Soc. London, Ser. A* **1954**, *225*, 71.

(35) Kim, Y.-K.; Irikura, K. K.; Rudd, M. E.; Ali, M. A.; Stone, P. M.; Chang, J.; Coursey, J. S.; Dragoset, R. A.; Kishore, A. R.; Olsen, K. J.; Sansonetti, A. M.; Wiersma, G. G.; Zucker, D. S.; Zucker, M. A. *Electron-Impact Cross Sections for Ionization and Excitation Database*. http://physics.nist.gov/PhysRefData/Ionization.

(36) Joshipura, K. N.; Vinodkumar, M.; Patel, U. M. *J. Phys. B: At., Mol. Opt. Phys.* **2001**, *34*, 509−519.

(37) Fitch, W. L.; Sauter, A. D. *Anal. Chem.* **1983**, *55*, 832−835.

(38) Cool, T. A.; Nakajima, K.; Taatjes, K. A.; McIlroy, A.; Westmoreland, P. R.; Law, M. E.; Morel, A. *Proc. Combust. Inst.* **2005**, *30*, 1681−1688.

(39) Gerasimov, I. E.; Knyazkov, D. A.; Yakimov, S. A.; Bolshova, T. A.; Shmakov, A. G.; Korobeinichev, O. P. *Combust. Flame* **2012**, *159*, 1840−1850.

(40) Korobeinichev, O. P.; Ilyin, S. B.; Mokrushin, V. V.; Shmakov, A. G. *Combust. Sci. Technol.* **1996**, *116−117*, 51−67.

(41) Kaskan, W. E. *Symp. Combust., [Proc.]* **1957**, *6*, 134−141.

(42) Shaddix, C. R. Correcting thermocouple measurements for radiation loss: a critical review. *Proceedings of the 33rd National Heat Transfer Conference, Albuquerque, NM*; American Society of Mechanical Engineers: New York, NY, 1999.

(43) Kee, R. J.; Grcar, J. F.; Smooke, M. D.; Miller, J. A. *A Fortran Program for Modeling Steady Laminar One-Dimensional Premixed Flames*; Sandia National Laboratories Report SAND85-8240; Sandia National Laboratories: Livermore, CA, 1985.

(44) Kee, R. J.; Rupley, F. M.; Miller, J. A. *Chemkin-II: A Fortran Chemical Kinetics Package for the Analysis of Gas-Phase Chemical Kinetics*; Sandia National Laboratories Report SAND89-8009; Sandia National Laboratories: Livermore, CA, 1989.

(45) Turanyi, T.; Zsely, I. G.; Frouzakis, C. KINALC: A CHEMKIN Based Program for Kinetic Analysis, 2007. http://respecth.chem.elte.hu/respecth/.

999 (46) Turanyi, T. Mechmod version 1.4: Program for the trans-
1000 formation of kinetic mechanisms, 2002. http://respecth.chem.elte.hu/
1001 respecth/.

1002 (47) Metcalfe, W. K.; Burke, S. M.; Ahmed, S. S.; Curran, H. J. *Int. J.*
1003 *Chem. Kinet.* **2013**, *45*, 638−675.

1004 (48) *SAUDI ARAMCO Mechanism Release*, v. 2.0; Combustion
1005 Chemistry Centre, National University of Ireland: Galway, 2016.
1006 http://c3.nuigalway.ie/aramco2/download.html.

1007 (49) Hori, M.; Matsunaga, N.; Marinov, N.; Pitz, W.; Westbrook, C.
1008 *Symp. Combust., [Proc.]* **1998**, *27*, 389−396.

1009 (50) Wang, H.; You, X.; Joshi, A.; Davis, S. G.; Laskin, A.;
1010 Egolfopoulos, F. N.; Law, C. K. USC Mech II; 2007. http://ignis.usc.
1011 edu/USC_mech_II.htm.